Spheroid models to elaborate the broken symmetry and equivalent volume of molecules in crystalline phase

Weihao Wang,[1] Zhenghong Chen,[1,2] Yang Gao,[2,3] Chenhao Chen,[1,2] Yang Jiao,[4] and Shaodong Zhang[1,*]

[1]*School of Chemistry and Chemical Engineering, Shanghai Jiao Tong University, Shanghai 200240, China*

[2]*Zhiyuan College, Shanghai Jiao Tong University, Shanghai 200240, China*

[3]*School of Mathematical Sciences, Shanghai Jiao Tong University, Shanghai 200240, China*

[4]*Materials Science and Engineering, Arizona State University, Tempe, Arizona 85287, USA*

(Received 25 August 2023; revised 11 April 2024; accepted 19 May 2024; published 6 June 2024)

Dense packing of particles has provided powerful models to elaborate the important structural features of matter in various systems such as liquid, glassy, and crystalline phases. The simplest sphere packing models can represent and capture salient properties of the building blocks for covalent, metallic, and ionic crystals; it, however, becomes insufficient to reflect the broken symmetry of the commonly anisotropic molecules in molecular crystals. Here, we develop spheroid models with a minimal degree of anisotropy, which serve as a simple geometrical representation for a rich spectrum of molecules—including both isotropic and anisotropic, convex and concave ones—in crystalline phases. Our models are determined via an inverse packing approach: Given a molecular crystal, an optimal spheroid model is constructed using a contact diagram, which depicts the packing relationship between neighboring molecules within the crystal. The spheroid models are capable of accurately capturing the broken symmetry and characterizing the equivalent volume of molecules in the crystalline phases. Moreover, our model retrieves such molecular information from low-quality x-ray diffraction data with poorly resolved structures, and by using soft spheroids, it can also describe the packing behavior in cocrystals.

DOI: 10.1103/PhysRevE.109.064603

I. INTRODUCTION

In the crystalline phase, the packing arrangement of individual building blocks (BBs), including atoms, ions, molecules [1,2], nanoparticles [3], and colloidal particles [4], to name but a few, plays a pivotal role in determining the properties of the matters that they form, which is therefore of great interest in the modern era of physical, chemical, and materials sciences [5,6]. Taking covalent, metallic, and ionic crystals, for instance, their structures have been successfully described by the sphere packing modeling, in which their corresponding BBs are represented by the simplest and fully isotropic geometrical shape [5], capturing salient fundamental properties of the BBs (such as symmetry). On the other hand, the sphere models are generally insufficient to describe complex molecular crystals, as the isotropic shape cannot reflect the broken symmetry of the molecules [illustrated in Fig. 1(a)]. Geometric representations with additional degrees of freedom are thus required for complex molecules to elucidate the molecular packing in the crystalline phases.

The study of particle packing with various shapes recently has attracted considerable attention. Dense packings of a variety of anisotropic particles including ellipsoids [7], tetrahedra [8], superballs [9,10], and polyhedral [11,12] have been investigated, as these nonspherical particles provide improved and more realistic representations of complex anisotropic BBs for a variety of condensed matters [13,14].

One approach of this research delves into the random packing of such particles within different environments. Anisotropic shapes, characterized by varying aspect ratios, are simulated to elucidate the densest packing configurations and the corresponding phase transitions [15–17]. Studies have revealed that the packing problem can be influenced either by excluded volume effects [18] or by crowding dynamics [19]. Various methods have been developed to simulate the packing density in random packing of diverse particles [20–22]. For example, equilibrium models of crowding were used to compute the packing fraction of randomly packed spheres, and such approaches can be further applied to anisotropic spheroids packing [23,24].

Another approach of this research focuses on packing within crystalline phases, wherein packing bodies are subjected to the constraints imposed by crystallographic symmetry [25–27]. Among these shapes, ellipsoids have long served to represent various types of BBs. For instance, an inertia-equivalent ellipsoid has been used as a low-resolution model for proteins, which facilitates the analysis of their surface properties [28–30]. Similarly, the ellipsoid of revolution model was employed to elucidate hydrodynamic effects, offering a simplified representation for macromolecules in solution [31,32]. In addition, dense packing of ellipsoids has found application in the study of organic crystals with low-symmetry compounds [33]. As a special type of ellipsoid, a spheroid exhibits symmetry-broken shape with the *minimal degree of anisotropy*, and yet they have demonstrated a rich spectrum of packing behaviors and were employed in the study of Frenkel-Mulder contact diagram [34], nematic phase transition [35],

*Contact author: sdzhang@sjtu.edu.cn

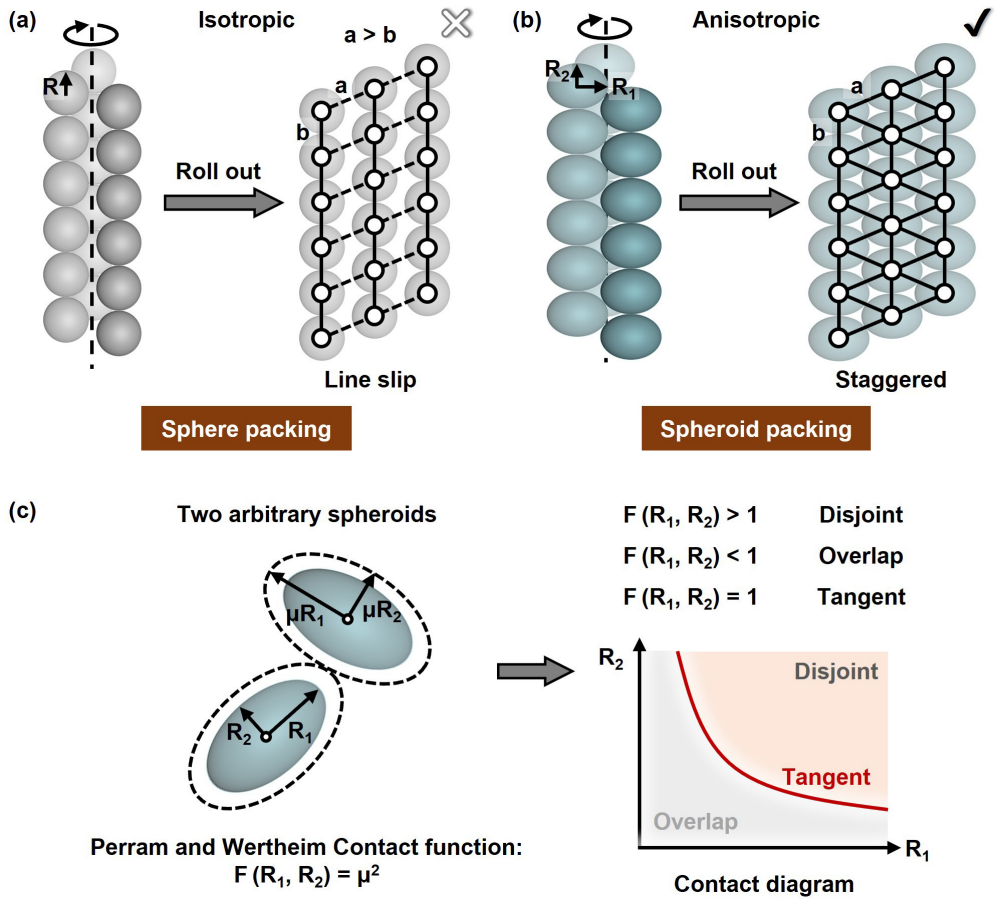

FIG. 1. Schematic illustration of anisotropy in molecular crystal packing and the construction of contact diagram. (a) Isotropic sphere packing model for common molecular crystals violates the close packing principle of crystallography, while (b) anisotropic spheroid packing model fulfills the dense packing. (c) Mathematical relationship between semiaxis R_1 and R_2 can be deduced from Perram and Wertheim contact function, with different regions of the contact diagram that correspond to different spatial relationship between spheroids.

and quasicrystals [36]. These intriguing studies imply that spheroids would also provide an effective representation for the equivalent volume of anisotropic complex BBs in the crystalline phase, i.e., the volume of the occupied space of each BB that is inaccessible by others. All these approaches use an ellipsoidal/spheroidal envelope to approximate the shape of molecules and provide useful information about single molecules. However, the contact between neighboring hard particles is insufficient to provide intermolecular information like dovetail between molecules, which requires the overlap of these geometric representations.

We herein report on a simple geometrical representation for complex molecules in crystalline phases based on spheroid particles, which can reveal equivalent volume and dovetail behavior of molecules (Fig. 1). Our models are determined via an inverse packing approach: Unlike traditional packing problems that focus on finding the optimal packing arrangement for a given particle shape, our inverse packing approach identifies the optimal spheroid shape [defined by the two semiaxes R_1 and R_2 in Fig. 1(b)] that represents the molecules, when knowing their position and direction in the crystalline phase. To achieve this goal, we devise a contact diagram which depicts the packing relationship (overlapping, contact, nontouching) of all representative spheroid pairs derived by the symmetry operations within a molecular crystal.

By investigating distinct types of molecular crystals, we demonstrate the spheroid model can successfully capture the broken symmetry and key features of the molecules in their crystalline phases. In this paper, we also provide a paradigm that complex BBs can be represented by simple shapes allowing overlapping, instead of sticking to hard particles with increasing shape complexity. Although omitting many complex molecular details, the spheroid models are capable of accurately characterizing the equivalent volume of molecules in the crystalline phases. This is in contrast to the widely used van der Waals (vdW) volume [37,38], which typically contains redundant structural information and requires nontrivial computation even for relatively simple molecules (such as CH_4). Our models are also effective even with poorly resolved crystals by x-ray diffraction. These data are usually caused by intrinsic molecular flexibility, inadequate crystal growth conditions, or low resolution of the x-ray diffractometer, which are otherwise considered invalid and simply discarded. With our method, valuable packing information from these low-quality data can be extracted as useful input for further optimization of molecular design. Additionally, our spheroid model can also be applied to cocrystals, in which the synergistic interplay between different components gives rise to unique properties. The spheroids in these crystals offer packing information between the complexes,

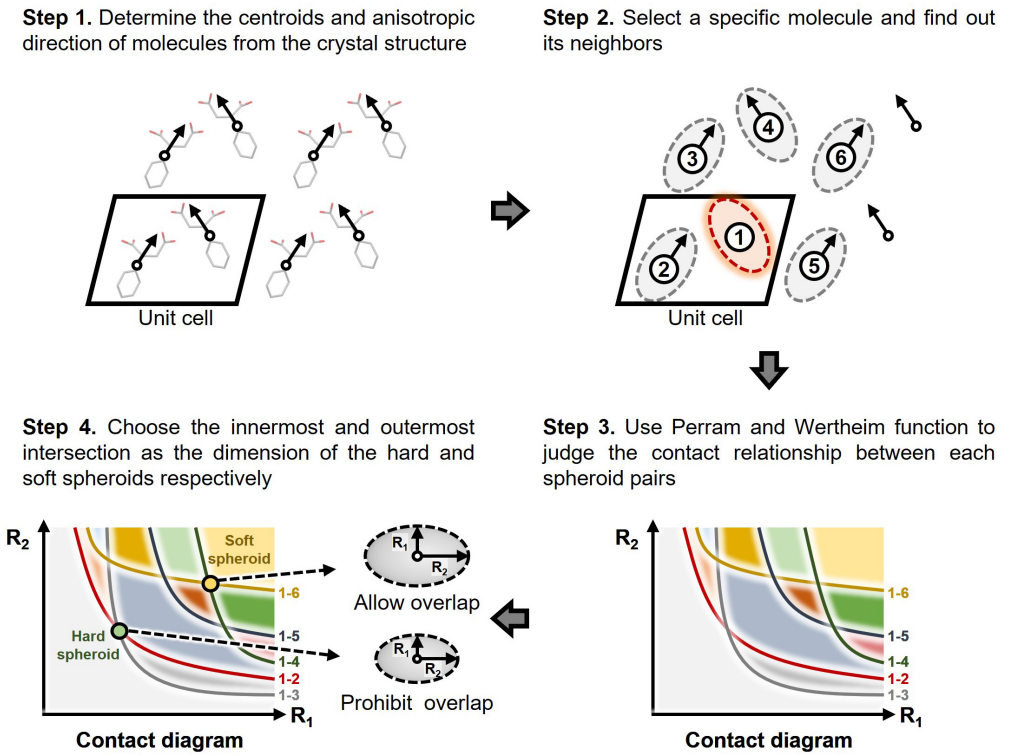

FIG. 2. Detail procedure for determining hard and soft spheroids. For a given molecular crystal, the position and direction of each molecule are first determined, corresponding to the centroid and axis of the spheroid, respectively. Varying the dimension of the spheroid, its spatial relationship with the neighbors is depicted in a contact diagram, and curves with different color show the relationships of different spheroid pairs. Finally, the innermost and outermost intersections in the contact diagram are chosen as the dimension of hard and soft spheroids, respectively.

thus providing insights into the rational design of cocrystal structures.

II. SPHEROID MODEL

It is worth noting that the main constraints of crystalline spheroid packing are not due to the confinement of space, which will impact its collective dynamics, such as viscosity, by affecting the motion of distant molecules [17]. We here focus on the symmetry operations in the crystal and use an inverse packing approach to derive the spheroid dimension from the known crystal structure. The detailed process is described as follows (Fig. 2): The centroid of a molecule is represented with the center of a spheroid, which is placed on a site of the molecular crystal lattice. The principal direction of the spheroid (i.e., direction of the axis of resolution of the spheroid) corresponds to that of the molecule, which is typically associated with the direction of molecular dipole moment. For a nonpolar molecule, its principal symmetry axis is used to align with the principal direction of the spheroid. Once the position and direction of spheroids are determined, the osculation of two adjacent spheroids can be described using the relationship between their respective semiaxes R_1 and R_2 [see Fig. 1(c) for illustration]. This R_1/R_2 correlation is derived according to the Perram and Wertheim contact function [39], which corresponds to a curve in the contact diagram. A contact diagram is therefore constructed with a series of contact curves, which depicts whether a pair of spheroids with a specific semiaxis ratio R_1/R_2 overlap, contact, or are mutually separated (illustrated in detail in Fig. 3). It in turn allows us to determine the dimension of spheroids that represents the equivalent volume of the molecules within the crystalline phase, as described in detail below.

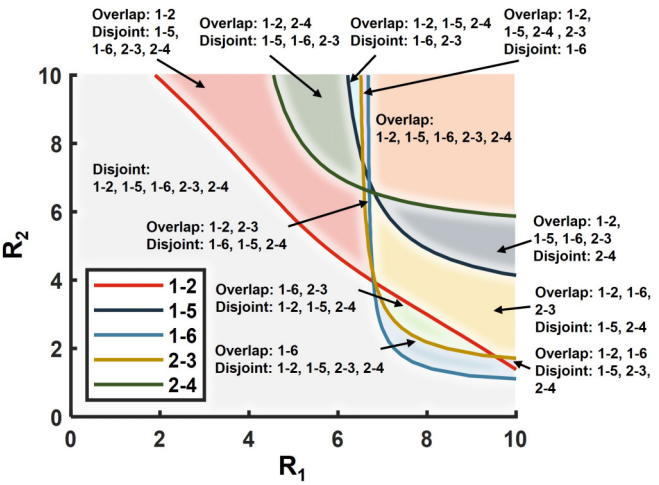

FIG. 3. Detailed contact diagram: a molecular cage crystal with space group $P2_1/n$.

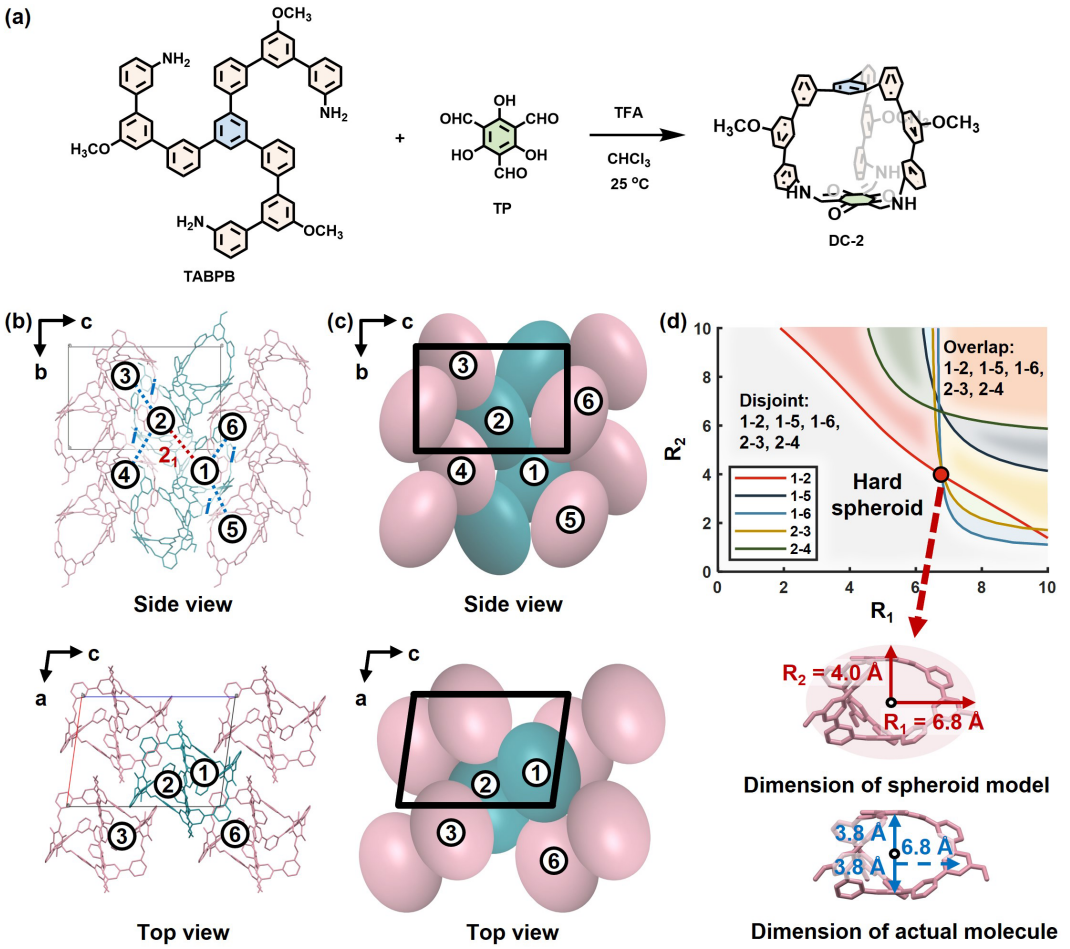

FIG. 4. Spheroid packing model for a crystal of cagelike molecules with space group $P2_1/n$. (a) Synthesis of the cagelike model compound DC-2. (b) Side and top views of the molecular packing in the crystalline phase. (c) Side and top views of simulated spheroid packing with magenta and cyan colors used for easy inspection. (d) Computed contact diagram of hard spheroid packing. Curves with different colors correspond to contacts between different pairs of molecules. Simulated hard spheroid shows similar dimension with that of the actual molecule.

A. Hard spheroid model applied to molecular crystal

As a class of molecules, cagelike compounds recently have attracted considerable attention [40–49]. By virtue of their rich geometric diversity, molecular cages can be used as promising BBs for the search of supramolecular materials that are hardly accessible by conventional molecules [50]. As a proof of concept, cage molecules with rigid and well-defined three-dimensional structure are first selected to demonstrate our spheroid model for molecular crystals. The spheroid packing is constructed by considering symmetry constraints imposed by the crystal lattice, which is first illustrated with a crystal formed by molecular cage DC-2 that we synthesized according our previous protocol (Fig. 4) [51]. Very briefly, it is formed by the reaction between 2,4,6-trihydroxybenzene-1,3,5-tricarbaldehyde and a triamino-functionalized TABPB, as illustrated in Fig. 4(a). Their detailed synthetic procedures, nuclear magnetic resonance, and matrix-assisted laser desorption/ionization time-of-flight analyses the detailed synthetic procedures and chemical characteristics are referred to our previous work [52].

In this crystal with space group of $P2_1/n$, a molecule is related to its neighbors through symmetry operations of inversion (i), screw (with 2_1 axis) and glide, with the latter a product of the first two operations. Therefore, we only need to consider inversion and screw symmetry constraints to construct a local cluster of spheroids, from which a contact diagram can be derived. To explain the contact imposed by twofold screw operations, two adjacent spheroids labeled as 1 and 2 on the screw axis are first selected. Each of the two spheroids further osculate two neighboring spheroids with inversion constraint, which are labeled from 3 to 6, respectively. As a result, only a local cluster of six spheroids is required to elucidate all contact relationships in such a case, as illustrated in Fig. 4(c).

Figure 4(b) reveals the crystal structure viewed along crystallographic a and b axes, and the packing of the corresponding spheroidal model is shown in Fig. 4(c). Taking the contact of spheroids 1 and 2, for instance, with their orientations and center positions fixed, R_1 and R_2 cannot vary independently while maintain the contact—they need to vary coherently, leading to a correlation between R_1 and R_2 depicted by the red line in the contact diagram in Fig. 4(d). The two spheroids are disjointed when the coordinate (R_1, R_2) is below of the line, while they are intercalated when the coordinate is above. By iterating the R_1/R_2 relationship with other spheroid pairs, all five lines reflecting their osculation

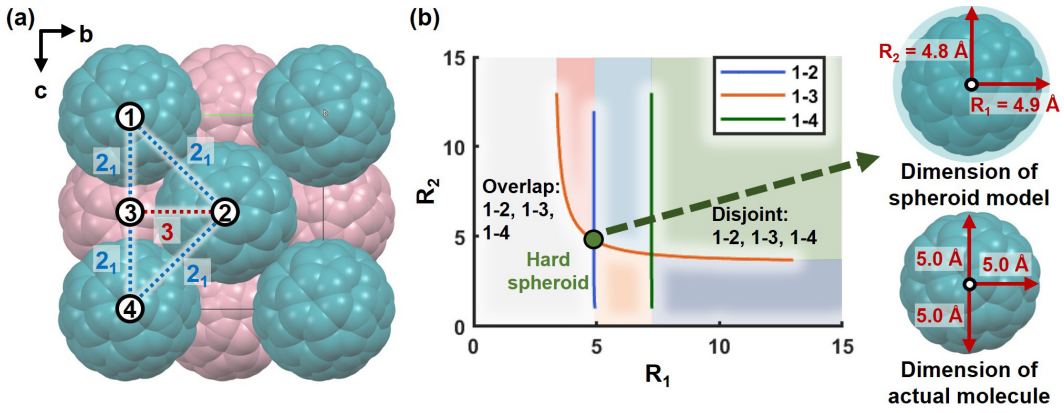

FIG. 5. Spheroid packing in fullerene crystal with space group *Pa*3. (a) Crystal structure viewed along the *a* axis. Adjacent molecules are related through different symmetry operations. (b) Computed contact diagram of spheroid packing. The simulated shape and dimension are close to those of a fullerene molecule.

are derived. As a result, the contact diagram is divided into various regions that correspond to different packing patterns. For example, the gray region in the bottom left area shows that all spheroids are disjointed, and the orange part on the top right corner indicates that all spheroids overlap with each other.

For hard spheroids, overlap is prohibited, and two arbitrary spheroids can only be tangent or disjointed to each other. As the leftmost intersection [red circle in Fig. 4(d)] reaches the largest contact number while guaranteeing no overlap of spheroids, this coordinate is therefore deemed as the dimension of the hard spheroid. Accordingly, the polar and equatorial radii of the spheroid are calculated to be 4.0 and 6.8 Å, respectively. This calculated dimension is almost identical to that of the actual molecule with a height of 7.6 Å and a radius of 6.8 Å.

This spheroid model can also be applied to the molecular crystals formed by (quasi)isotropic molecules, which is exemplified with landmark molecule fullerene C_{60} with large void [53]. The vdW volume only counts the sum of the occupied space of all atoms but excludes the cavity and thus cannot accurately characterize the equivalent volume of such type of molecules in dense crystalline packing. As illustrated in Fig. 5, the molecular crystal (space group *Pa*3) is constrained by the screw operation (with 2_1 axis) and rotation (threefold axis). Therefore, only four spheroids are required to describe all the contact relationships in Fig. 5(a), which correspond to three contact lines of 1–2, 1–3, and 1–4 spheroid pairs. Similarly, the coordinate of the leftmost intersection (in red circle) refers to the two semiaxes of the hard spheroid, i.e., 4.9 and 4.8 Å, respectively [Fig. 5(b)]. These values are in good accordance with the radius of a fullerene in the crystalline phase.

B. Applicability and generality of hard spheroid model

We subsequently verified the applicability and generality of the spheroid model with a variety of randomly selected molecules with regular shape (Table I). To this end, we compared our hard spheroid model with the conventional space-filling vdW model, both of which were used to probe the equivalent volume of molecules in the crystalline phase (Fig. 6). Seventeen extra molecules including peptides, cholesterols, triptycene, macrocycles, and other small molecules were analyzed, with their contact diagrams shown in Figs. S1–S4 in the Supplemental Material [62], and their vdW volumes were calculated with the multifunctional program Multiwfn [54].

As shown in Fig. 6, the data points close to the yellow line indicate similar values of volume in the two models. Different colors of the data points indicate different types of molecules: General molecules with regular shape are shown in blue, red dots represent compounds with cavity, and purple symbols stand for some seriously dovetailing molecules.

Focusing on the enlarged area in Fig. 6, we can find that the hard spheroid volume is fairly close to the vdW volume for relatively small and regular molecules. This is because these molecules are compact and do not interpenetrate in their crystalline packings, and both the space-filling and spheroid models are applicable. However, for porous molecules, their intrinsic cavity is considered by the hard spheroid model, whose dimension is thus larger than the corresponding vdW volume that does not consider the cavity. Our spheroid model therefore can better describe the equivalent volume of such molecules. Moreover, for the molecules with concave structure and/or flexible fragments, they are often prone to dovetail with each other during molecular packing. This information, particularly the penetration percentage, can hardly be unraveled by the vdW model. In the hard spheroid model, overlap between spheroids is forbidden, and the calculation of spheroid volume will exclude the dovetailed part, causing an underestimation of the equivalent volume. To address this problem, the soft spheroid model is proposed, which can depict the dovetail through interpenetration percentage between the spheroids (*vide infra*).

C. Soft spheroid model for dovetailed molecules

We further examined a ubiquitous type of molecules that dovetail with each other during crystallization. This is first showcased with our recently reported twin-cavity cage [55]. Figure 7(a) manifests the molecular packing viewed along the *c* axis in the crystal (space group $P3_221$). As their packing is imposed by symmetry operations of screw (with 3_2 and

TABLE I. The calculated hard spheroid volume and vdW volume of 17 different molecules collected from Cambridge Crystallographic Data Centre (CCDC).

Compound	CCDC number	Space group	Hard spheroid volume (Å^3)	VdW volume (Å^3)
Small molecule	202500	$P\bar{1}$	110	190
Small molecule	1133112	Cc	139	148
Triethylenediamine	1269548	$P6_3/m$	118	108
Ferrocene	1154857	$P2_1/a$	152	125
Cortisone	2010417	$P2_12_12_1$	221	323
Cholic acid	1116202	$P2_1$	396	381
Helicene	1521681	$P2_12_12_1$	259	287
Triptycene	1275698	$P2_12_12_1$	175	210
Corannulene derivative	1567460	$P3c1$	2424	2439
Vitamin B12	1944201	$P2_12_12_1$	1357	1120
Chainlike molecule	257085	$P\bar{1}$	1055	1434
Peptides	1190276	$P2_1$	146	443
Macrocycle	1822570	$P2_1/c$	556	555
Macrocycle	1950613	$R\bar{3}$	952	1255
Cage	1453937	$R\bar{3}c$	2063	1592
Cage	1566755	$C2/c$	2364	2031
$C_{76}Cl_{16}$	650718	$Pbca$	701	934

2_1 axes) and rotation (twofold axis), five different spheroids labeled from 1 to 5 are selected accordingly.

Like the aforementioned analysis, the hard spheroid corresponds to the intersection of dark blue and yellow lines in the contact diagram in Fig. 7(c), corresponding to a spheroid with polar and equatorial radii of 6.3 and 6.2 Å, respectively. However, compared with the actual dimension of the molecule, the hard spheroid obviously contracts, as pictured in Fig. 7(d). This is because the compounds are indeed interpenetrated in the crystalline phase, and the use of hard spheroid model unavoidably excludes the dovetailed part, which therefore underestimates the equivalent volume of such molecules.

To better delineate the interpenetration of this class of molecules, we introduced a supplementary soft (i.e., overlapping) spheroid model [56]. Unlike hard spheroids, soft spheroids are elastic and allow deformation so that all spheroids of interest are either contacting or overlapping. It means their disconnection is avoided, and the soft spheroid packing in this crystal is displayed in Fig. 7(b). Accordingly, the outermost node is the critical point for reaching the largest contact number, which is chosen as the coordinate for presenting the dimension for the soft spheroid [Fig. 7(c)]. Notably, if there is more than one innermost or outermost node, the one with the largest value of $R_1^2R_2$ is chosen. This is because this value corresponds to the largest spheroid volume, complying with the highest packing fraction in the crystalline phase. Additionally, overlap of spheroids is forbidden by translation operation, as it is not consistent with the dovetailing of the particles. The largest polar and equatorial radii of the soft spheroid are therefore calculated to be 17.1 and 8.8 Å, respectively; the interpenetration percentage is ∼26%, while the dovetail of actual molecules is ∼25%, as shown in Fig. 7(d). Indeed, the hard and soft spheroids respectively determine the lower and upper limits of the equivalent dimension for a

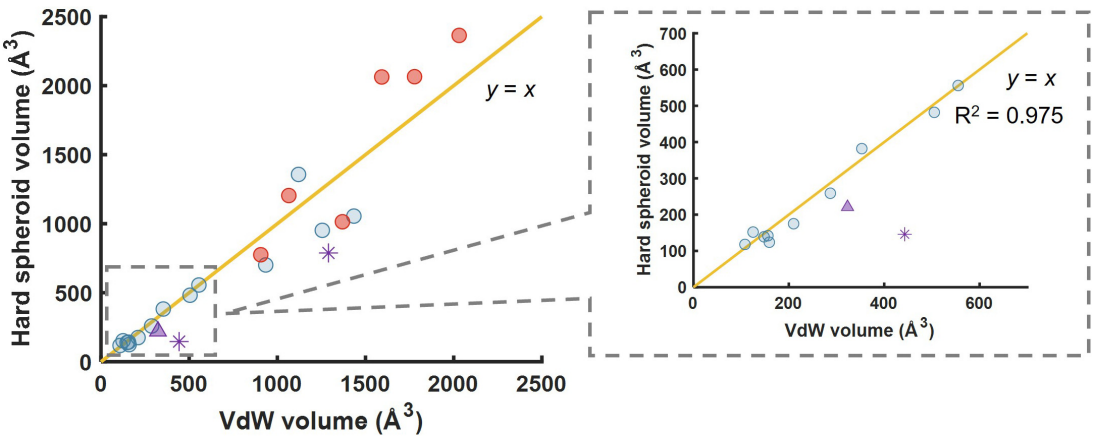

FIG. 6. Comparison of simulated hard spheroid volume and van der Waals (vdW) volume of a wide spectrum of complex molecules. Red dots represent molecules with cavity, purple asterisks represent situations for severely dovetailed molecules that will be addressed with soft spheroid models, and blue dots represent other molecules. Enlarged is the simulated hard spheroid volume of small molecules showing good linear relationship with their vdW volume.

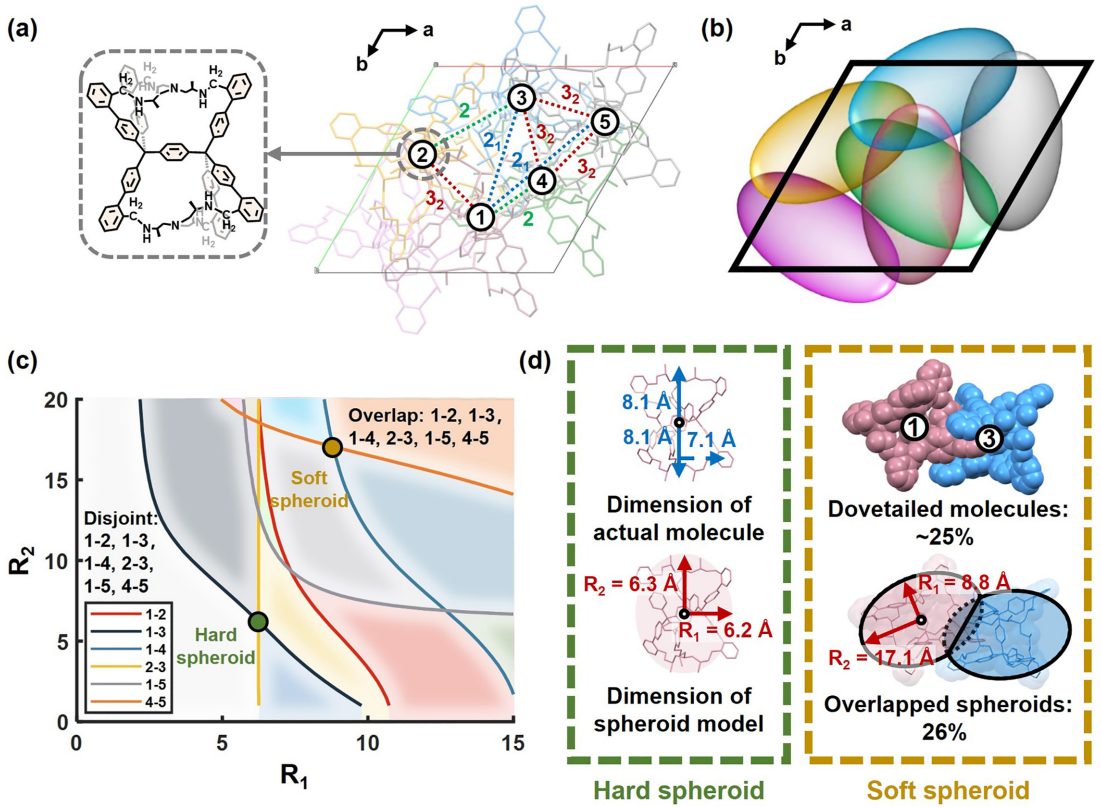

FIG. 7. Spheroid packing in a crystal (space group $P3_221$) formed by dovetailing twin-cavity cages. (a) Crystal structure viewed along the c axis. Adjacent molecules are constrained by symmetry operations. (b) Simulated soft spheroid packing; (c) Computed contact diagram of spheroid packing. The innermost node represents hard spheroid, while the outermost node represents soft spheroid. (d) Calculated hard spheroid is smaller than actual molecule, and soft spheroid reflects the dovetail between molecules based on the overlap percentage.

specific molecule in the crystalline phase, and the most suitable shape model should depend on the convexity/concavity of the molecule.

III. SCOPE OF SPHEROID MODEL

A. Application to poorly resolved crystal

For crystals with good quality, we can deduce molecular information including molecular centroids and vdW volume through x-ray diffraction data. However, in cases of poor-quality crystals where atoms may be omitted or incorrectly connected due to low resolution of the crystal x-ray diffraction data, the derived molecular information is typically deemed invalid and disregarded.

Indeed, we further demonstrated that our spheroid model can effectively explore the molecular packing of such imperfect crystals with incomplete structural refinement. It enables the capture of valuable insight into equivalent volume and dovetail behavior, thus salvaging meaningful information from otherwise discarded data.

Illustrated in Fig. 8 is the contact diagram derived from the poorly resolved crystalline phase of the molecules used in Fig. 1. This rough structure was obtained from original crystal data without further refinements, with an R-factor of ∼39% [57]. The semiaxes of the simulated spheroid were determined to be 6.8 and 3.7 Å, respectively, which are close to the spheroid dimension calculated from the precise structure. Our spheroid model, therefore, can provide a tool for extracting valuable information of molecular packing in crystals of low quality, which would be useful input for the optimization of molecular design.

B. Application to cocrystals

Recently, the rational design of molecular cocrystals with two or more components has attracted consideration attention

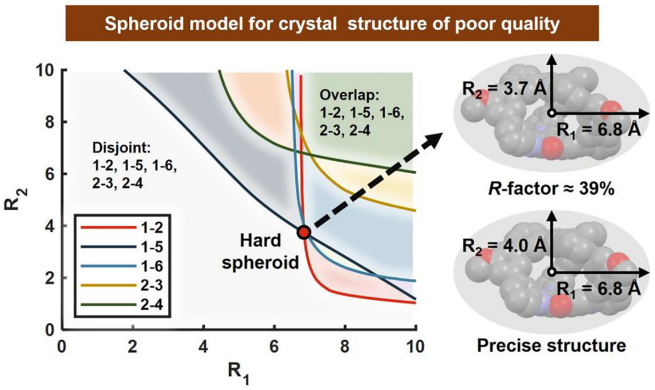

FIG. 8. Spheroid model applied in poor-quality crystals. The contact diagram is derived from the rough structure (R-factor ∼ 39%) and its simulated spheroid is close to the spheroid calculated from precise structure. The quality of the refined crystal structures is usually considered acceptable when $R \leqslant 0.05$ for small organic molecules and $R \sim 0.20$ for complex systems like proteins.

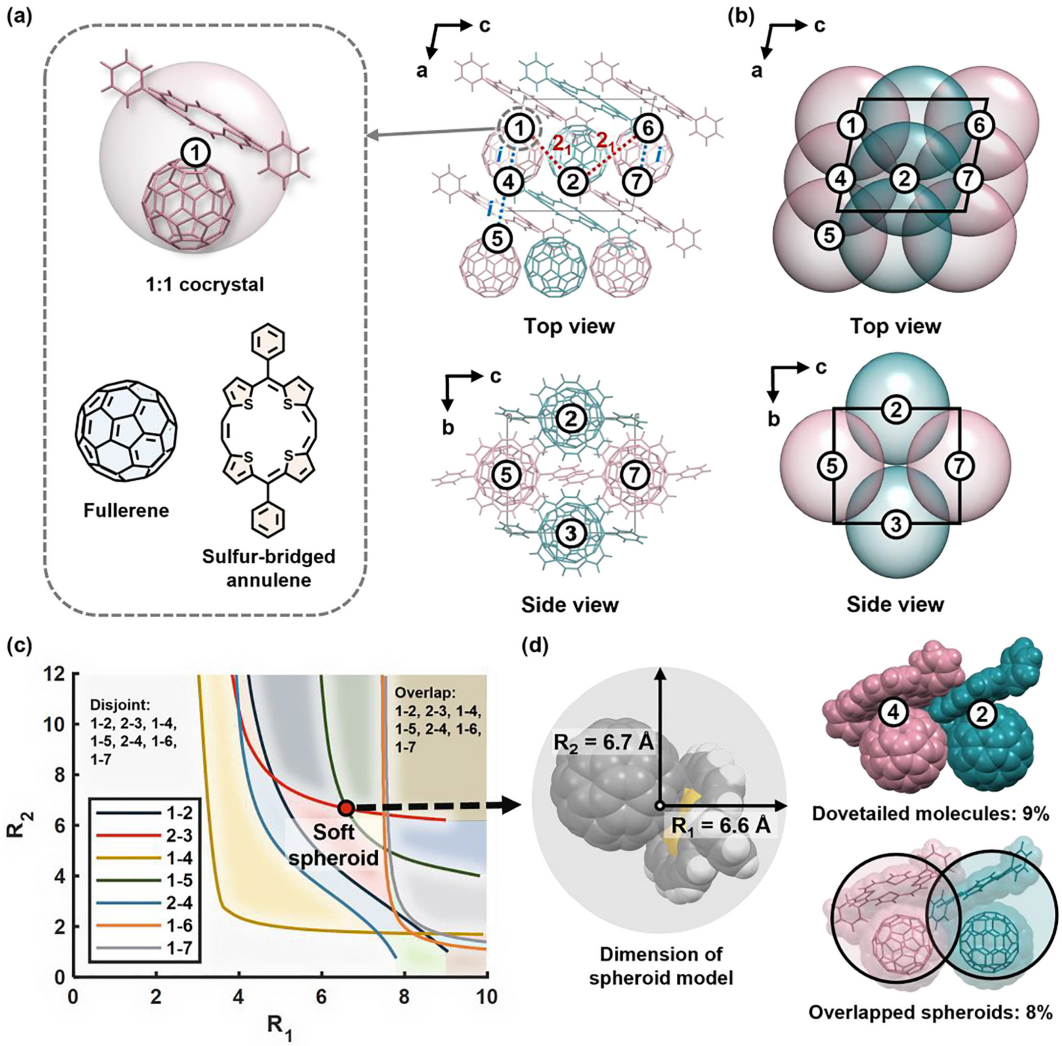

FIG. 9. Spheroid packing in cocrystal with space group $P2_1/c$. (a) Crystal structure viewed along the b and a axes. A simulated spheroid includes one fullerene molecule and one annulene molecule. (b) Simulated soft spheroid packing. (c) Computed contact diagram of spheroid packing. (d) The dimension of the calculated soft spheroid. Soft spheroid can reflect the dovetail between different complexes based on the overlap percentage.

in the field of materials science [58–60]. As compared with the individual components, the properties of these cocrystals can be dramatically different, which stem from the synergistic interplay between the components. Understanding the packing behavior in cocrystals thus provides a guidance to realize the desired properties. When studying the molecular packing in cocrystals based on our model, it is common for spheroids to contain more than one molecule. In these cases, the polar axis of a spheroid represents the anisotropic direction of the molecular complex, rather than a single molecule. Furthermore, since the symmetry of the molecules may coincide with the symmetry of the crystal, it is possible for one molecule to be shared by different complexes. For this reason, soft spheroids are a more appropriate model for describing the packing behavior in the cocrystals.

To this end, a 1:1 fullerene/sulfur-bridged annulene cocrystal [61] (space group $P2_1/c$) is analyzed as an example (Fig. 9), and the spheroid should include the nearest pair of these two molecules. Because both molecules are centrosymmetric and located at the inversion center of the crystal, a single molecule is shared by two different complexes, as shown in Fig. 9(a). Like the aforementioned analysis process, seven spheroids labeled from 1 to 7 are selected, and their contact diagram is shown in Fig. 9(c). The soft spheroid corresponds to the intersection of the red and green lines, as the overlap of spheroids is prohibited for translation symmetry operations. Therefore, as displayed in Fig. 9(d), the equatorial and polar radii of the simulated soft spheroid are ∼6.6 and 6.7 Å, respectively. Moreover, the application of soft spheroid packing also provides information about the dovetail between adjacent complexes. For instance, the dovetail between actual complexes 2 and 4 is ∼9%, while soft spheroids give a calculated overlap percentage of 8%. The simulated soft spheroid packing pattern in this cocrystal is finally suggested in Fig. 9(b).

IV. CONCLUSIONS

Ellipsoidal and spheroidal shapes have long been used as anisotropic geometric representations of complex molecules

for studying their packing behaviors, including random packing and ordered packing in the crystalline phase. These models provide useful information of single molecules; they are yet to offer intermolecular information, as they rather deal with the contact between hard particles.

In this paper, a spheroid model has been developed to probe molecular packing in molecular crystals. The hard and soft spheroids, prohibiting and allowing overlap, respectively, omit the detailed complexity of the molecules but successfully retrieve packing information of equivalent volume and molecular dovetail. Moreover, it is demonstrated that our low-resolution spheroid model, compared with conventional space-filling model, shows a tolerance of crystal quality and can also be applied to cocrystal systems. We expect our model can be readily generalized to more complex molecular crystals by increasing the degrees of freedom of the fundamental geometric representation, e.g., from spheroid to generic ellipsoid or other shapes, which we will explore in our future work.

ACKNOWLEDGMENTS

We are grateful for financial support from the National Natural Science Foundation of China (Grants No. T2325017, No. 92356306, No. 22271187, and No. 22071153), the Science and Technology Commission of Shanghai Municipality (Grant No. 21JC1401700) and the Zhiyuan Future Scholar Program (Grants No. ZIRC2022-18). The crystallographic experiments were conducted with beam line BL17B1 supported by Shanghai Synchrotron Radiation Facility.

W.W. and S.Z. designed this work. W.W. and Y.G. built the mathematical model of spheroid packing. W.W., Z.C., and C.C. collected and analyzed the data. W.W., Y.J., and S.Z. discussed the results and prepared the paper.

APPENDIX A: COMPUTATIONAL METHODS OF HARD AND SOFT SPHEROID MODELS

We take the Perram-Wertheim contact function to probe the spatial relationship between spheroids. This function reveals the correlation between spheroid position, orientation, dimension, and osculation. First, the position and direction information of a spheroid can be determined by the specific crystal lattice, which is provided by the Cambridge Structural Database. Next, we assume two spheroids osculate with each other, which is realized by adjusting R_1 and R_2 to ensure that the value of contact function is $\sim$1. Every osculation of a spheroid pair will therefore correspond to a curve in the contact diagram, showing the variation of R_1 and R_2. As only limited symmetry operations are present in a crystal, the sort of packing relationship (overlapping, contact, nontouching) between adjacent spheroids is also finite. Therefore, we only need to analyze those representative spheroids pairs that contain all contact relationships in a crystal. As a result, the contact diagram consists of several curves that reflect the osculation of different spheroid pairs, and these curves divide the diagram into various sections representing different packing relationships of spheroids.

The selected hard and soft spheroids, prohibiting or allowing overlap, respectively, correspond to the leftmost and rightmost intersections. Therefore, the volume of hard spheroid can be easily determined by MATLAB, which is then compared with its vdW volume calculated by Multiwfn. Additionally, the interpenetration percentage of soft spheroids, defined as the quotient of overlapped volume and soft spheroid volume, is derived by Monte Carlo algorithm and is used to describe the dovetail between molecules with concave structure or flexible fragments.

APPENDIX B: SELECTION OF THE REPRESENTATIVE SPHEROID PAIRS

Representative spheroids that can depict all contact relationships in a crystal are first selected, based on which the contact diagram is derived. To explain the principle of the selection of these spheroids, the monoclinic crystal mentioned in this paper with space group $P2_1/n$ is taken as an example (Fig. 4). The main symmetry operations of this space group are inversion, twofold screw rotation, and glide. If we have any two of them, the third operation is the combination product of the first two. Therefore, we only consider osculation under inversion and screw rotation operations in this instance for convenience. To depict the constraint under twofold screw rotation, only two spheroids labeled 1 and 2 are required. Each of the two spheroids further osculate two neighboring spheroids imposed by inversion, which are labeled from 3 to 6, respectively. It leads to the identification of spheroid pairs 1–5, 1–6, 2–3, and 3–4, which are used to reflect the contact relationship constrained by inversion operation. As a result, we only need to study the packing relationship between six spheroids as a local cluster in this crystal.

As shown in Fig. 10, the polar direction of spheroids under inversion and translation operations are consistent, and the mathematical expressions of their osculation are given by Eqs. (B1) and (B2), respectively:

$$\frac{{d_1}^2\cos^2\theta_1}{4{R_2}^2}+\frac{{d_1}^2\sin^2\theta_1}{4{R_1}^2}=1, \tag{B1}$$

$$\frac{{d_2}^2\cos^2\theta_2}{4{R_2}^2}+\frac{{d_2}^2\sin^2\theta_2}{4{R_1}^2}=1. \tag{B2}$$

In this crystal, the values of these parameters are measured in Eq. (B3):

$$d_1 = 13.2\,\text{Å}, \quad \theta_1 = 77.8^\circ, \quad d_2 = 16.4\,\text{Å}, \quad \theta_2 = 60.1^\circ. \tag{B3}$$

We can observe that ${d_1}^2\cos^2\theta_1$ is smaller than ${d_2}^2\cos^2\theta_2$, and ${d_1}^2\sin^2\theta_1$ is also smaller than ${d_2}^2\sin^2\theta_2$. Therefore, if

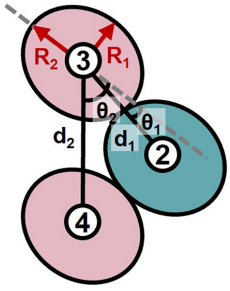

FIG. 10. Osculation under translation and inversion constraints.

two spheroids are in contact under translation constraints in this situation, spheroids through inversion operation will inevitably overlap. As a result, the screw rotation and inversion constraints of six spheroids are studied, while the translation constraints are ignored in the discussion of hard spheroids in this crystal.

APPENDIX C: CONTACT DIAGRAM

Illustrated in Fig. 3 is the detailed contact diagram of the abovementioned molecular crystal. Areas with different colors represent different packing relationships of spheroids. For instance, the red section means spheroids 1 and 2 are overlapped, while other spheroids are all disjointed. Coincidently, in this crystal, the red, golden, and cyan lines approximately meet at one point, which corresponds to the hard spheroid dimension. Therefore, the simulated hard spheroid packing pattern is described as: Spheroid 1 contacts with spheroids 2 and 6, spheroid 2 osculates with spheroid 3, and other spheroids are disjointed.

Moreover, the contact diagrams of 17 extra molecules are analyzed and shown in Figs. S1–S4 in the Supplemental Material [62] with their Cambridge Crystallographic Data Centre number listed below in each diagram. These examples display a wide variety of molecules, including peptides, hormone, fullerene, triptycene, macrocycles and vitamin. The diversity of the molecules provides reliable basis of manifesting molecule equivalent volume through our spheroid packing model.

[1] W. Han, P. Huang, L. Li, F. Wang, P. Luo, K. Liu, X. Zhou, H. Li, X. Zhang, Y. Cui *et al.*, Two-dimensional inorganic molecular crystals, Nat. Commun. **10**, 4728 (2019).

[2] E. Ahmed, D. P. Karothu, M. Warren, and P. Naumov, Shape-memory effects in molecular crystals, Nat. Commun. **10**, 3723 (2019).

[3] W. Mickelson, S. Aloni, W.-Q. Han, J. Cumings, and A. Zettl, Packing C_{60} in boron nitride nanotubes, Science **300**, 467 (2003).

[4] G. Wu, H. Cho, D. A. Wood, A. D. Dinsmore, and S. Yang, Confined assemblies of colloidal particles with soft repulsive interactions, J. Am. Chem. Soc. **139**, 5095 (2017).

[5] L. Pauling, *The Nature of the Chemical Bond* (Cornell University, Ithaca, 1960).

[6] S. Torquato, Perspective: Basic understanding of condensed phases of matter via packing models, J. Chem. Phys. **149**, 020901 (2018).

[7] A. Donev, I. Cisse, D. Sachs, E. A. Variano, F. H. Stillinger, R. Connelly, S. Torquato, and P. M. Chaikin, Improving the density of jammed disordered packings using ellipsoids, Science **303**, 990 (2004).

[8] A. Haji-Akbari, M. Engel, A. S. Keys, X. Zheng, R. G. Petschek, P. Palffy-Muhoray, and S. C. Glotzer, Disordered, quasicrystalline and crystalline phases of densely packed tetrahedra, Nature (London) **462**, 773 (2009).

[9] Y. Jiao, F. H. Stillinger, and S. Torquato, Optimal packings of superballs, Phys. Rev. E **79**, 041309 (2009).

[10] K. M. Salerno, D. S. Bolintineanu, G. S. Grest, J. B. Lechman, S. J. Plimpton, I. Srivastava, and L. E. Silbert, Effect of shape and friction on the packing and flow of granular materials, Phys. Rev. E **98**, 050901(R) (2018).

[11] S. Torquato and Y. Jiao, Dense packings of the platonic and Archimedean solids, Nature (London) **460**, 876 (2009).

[12] P. Kubala, Random sequential adsorption of platonic and Archimedean solids, Phys. Rev. E **100**, 042903 (2019).

[13] G. Grosso and G. P. Parravicini, *Solid State Physics* (Academic Press, Oxford, 2014).

[14] S. V. Franklin and M. D. Shattuck, *Handbook of Granular Materials* (CRC Press, Boca Raton, 2015).

[15] P. Bolhuis and D. Frenkel, Tracing the phase boundaries of hard spherocylinders, J. Chem. Phys. **106**, 666 (1997).

[16] A. Mughal, J. Winkelmann, D. Weaire, and S. Hutzler, Columnar structures of soft spheres: Metastability and hysteresis, Phys. Rev. E **98**, 043303 (2018).

[17] L. Sironi, G. Macetti, and L. Lo Presti, Molecular dynamics investigation of benzoic acid in confined spaces, Phys. Chem. Chem. Phys. **25**, 28006 (2023).

[18] P. van der Schoot, *Molecular Theory of Nematic (and Other) Liquid Crystals* (Springer, Cham, 2022).

[19] S. Rocks and R. S. Hoy, Structure of jammed ellipse packings with a wide range of aspect ratios, Soft Matter **19**, 5701 (2023).

[20] C. Song, P. Wang, and H. A. Makse, A phase diagram for jammed matter, Nature (London) **453**, 629 (2008).

[21] Y. Kallus, The random packing density of nearly spherical particles, Soft Matter **12**, 4123 (2016).

[22] F. M. Schaller, M. Neudecker, M. Saadatfar, G. W. Delaney, G. E. Schröder-Turk, and M. Schröter, Local origin of global contact numbers in frictional ellipsoid packings, Phys. Rev. Lett. **114**, 158001 (2015).

[23] A. Zaccone, Explicit analytical solution for random close packing in $d = 2$ and $d = 3$, Phys. Rev. Lett. **128**, 028002 (2022).

[24] C. Anzivino, M. Casiulis, T. Zhang, A. S. Moussa, S. Martiniani, and A. Zaccone, Estimating random close packing in polydisperse and bidisperse hard spheres via an equilibrium model of crowding, J. Chem. Phys. **158**, 044901 (2023).

[25] Y. Kallus and V. Elser, Dense-packing crystal structures of physical tetrahedra, Phys. Rev. E **83**, 036703 (2011).

[26] C. Jennings, M. Ramsay, T. Hudson, and P. Harrowell, Packing concave molecules in crystals and amorphous solids: On the connection between shape and local structure, Mol. Phys. **113**, 2755 (2015).

[27] M. Klues and G. Witte, Crystalline packing in pentacene-like organic semiconductors, CrystEngComm. **20**, 63 (2018).

[28] W. R. Taylor, J. M. Thornton, and W. G. Turnell, An ellipsoidal approximation of protein shape, J. Mol. Graph. **1**, 30 (1983).

[29] J. J. Müller and H. Schrauber, The inertia-equivalent ellipsoid: A link between atomic structure and low-resolution models of small globular proteins determined by small-angle X-ray scattering, J. Appl. Cryst. **25**, 181 (1992).

[30] B. Shiffman, S. Lyu, and G. S. Chirikjian, Mathematical aspects of molecular replacement. V. Isolating feasible regions in motion spaces, Acta Cryst. A **76**, 145 (2020).

[31] S. E. Harding and A. J. Rowe, Modelling biological macromolecules in solution: 1. The ellipsoid of revolution, Int. J. Biol. Macromol. **4**, 160 (1982).
[32] S. E. Harding, On the hydrodynamic analysis of macromolecular conformation, Biophys. Chem. **55**, 69 (1995).
[33] D. Ito, R. Shirasawa, Y. Iino, S. Tomiya, and G. Tanaka, Estimation and prediction of ellipsoidal molecular shapes in organic crystals based on ellipsoid packing, PLoS One **15**, e0239933 (2020).
[34] D. Frenkel, B. M. Mulder, and J. P. McTague, Phase diagram of a system of hard ellipsoids, Phys. Rev. Lett. **52**, 287 (1984).
[35] S. Heymans and T. Schilling, Elastic properties of the nematic phase in hard ellipsoids of short aspect ratio, Phys. Rev. E **96**, 022708 (2017).
[36] W. Jin, Y. Jiao, L. Liu, Y. Yuan, and S. Li, Dense crystalline packings of ellipsoids, Phys. Rev. E **95**, 033003 (2017).
[37] R. B. Corey and L. Pauling, Molecular models of amino acids, peptides, and proteins, Rev. Sci. Instrum. **24**, 621 (1953).
[38] A. Bondi, van der Waals volumes and radii, J. Phys. Chem. **68**, 441 (1964).
[39] J. W. Perram and M. S. Wertheim, Statistical mechanics of hard ellipsoids. I. Overlap algorithm and the contact function, J. Comput. Phys. **58**, 409 (1985).
[40] D. M. Kaphan, M. D. Levin, R. G. Bergman, K. N. Raymond, and F. D. Toste, A supramolecular microenvironment strategy for transition metal catalysis, Science **350**, 1235 (2015).
[41] H. Takezawa, K. Shitozawa, and M. Fujita, Enhanced reactivity of twisted amides inside a molecular cage, Nat. Chem. **12**, 574 (2020).
[42] C. Chen, Y. Sun, Y. Zhao, R. T. VanderLinden, W. Tuo, F. Zhang, S. Zhang, H. Sepehrpour, C. Yan *et al.*, Anthracene-induced formation of highly twisted metallacycle and its crystal structure and tunable assembly behaviors, Proc. Natl. Acad. Sci. USA **118**, e2102602118 (2021).
[43] X. Wang, Y. Wang, H. Yang, H. Fang, R. Chen, Y. Sun, N. Zheng, K. Tan, X. Lu, Z. Tian *et al.*, Assembled molecular face-rotating polyhedral to transfer chirality from two to three dimensions, Nat. Commun. **7**, 12469 (2016).
[44] C. Zhang, H. Wang, J. Zhong, Y. Lei, R. Du, Y. Zhang, L. Shen, T. Jiao, Y. Zhu, H. Zhu *et al.*, A mutually stabilized host-guest pair, Sci. Adv. **5**, eaax6707 (2019).
[45] L. Zhang, Y. Jin, G.-H. Tao, Y. Gong, Y. Hu, L. He, and W. Zhang, Desymmetrized vertex design toward a molecular cage with unusual topology, Angew. Chem. Int. Ed. **59**, 20846 (2020).
[46] J. Koo, I. Kim, Y. Kim, D. Cho, I.-C. Hwang, R. D. Mukhopadhyay, H. Song, Y. H. Ko, A. Dhamija, H. Lee *et al.*, Gigantic porphyrinic cages, Chem. **6**, 3374 (2020).
[47] Z. Yang, C. Yu, L. Chen, P. Li, J. Chen, K. J. Wu, Q. Zhu, Y.-Q. Zhao, X. Liu, and S. Zhang, A class of organic cages featuring twin cavities, Nat. Commun. **12**, 6124 (2021).
[48] W. Zhang, L. Chen, S. Dai, C. Zhao, C. Ma, L. Wei, M. Zhu, S. Y. Chong, H. Yang, L. Liu *et al.*, Reconstructed covalent organic frameworks, Nature (London) **604**, 72 (2022).
[49] B. P. Benke, T. Kirschbaum, J. Graf, J. H. Gross, and M. Mastalerz, Dimeric and trimeric catenation of giant chiral [8 + 12] imine cubes driven by weak supramolecular interactions, Nat. Chem. **15**, 413 (2023).
[50] G. R. Desiraju, Supramolecular synthons in crystal engineering—A new organic synthesis, Angew. Chem. Int. Ed. Engl. **34**, 2311 (1995).
[51] X. Liu, G. Zhu, D. He, L. Gu, P. Shen, G. Cui, S. Wang, Z. Shi, D. Miyajima, S. Wang *et al.*, Guest-mediated hierarchical self-assembly of dissymmetric organic cages to form supramolecular ferroelectrics, CCS Chem. **4**, 2420 (2022).
[52] Y. Zuo, X. Liu, E. Fu, and S. Zhang, A Pair of interconverting cages formed from achiral precursors spontaneously resolve into homochiral conformers, Angew. Chem. Int. Ed. **62**, e202217225 (2023).
[53] H. W. Kroto, J. R. Heath, S. C. Obrien, R. F. Curl, and R. E. Smalley, C_{60}: Buckminsterfullerene, Nature (London) **318**, 162 (1985).
[54] T. Lu and F. Chen, Multiwfn: A multifunctional wavefunction analyzer, J. Comput. Chem. **33**, 580 (2012).
[55] J. Chen, Z. Yang, G. Zhu, E. Fu, P. Li, F. Chen, C. Yu, S. Wang, and S. Zhang, Heterochiral diastereomer-discriminative diphanes that form hierarchical superstructures with nonlinear optical properties, JACS Au **2**, 1661 (2022).
[56] J. Winkelmann, B. Haffner, D. Weaire, A. Mughal, and S. Hutzler, Simulation and observation of line-slip structures in columnar structures of soft spheres, Phys. Rev. E **96**, 012610 (2017).
[57] *R*-factor measures the agreement between refined crystallographic model and experimentally observed diffraction data. The quality of the refined crystal structures is usually considered acceptable when $R \leqslant 0.05$ for small organic molecules and $R \sim 0.20$ for complex systems like proteins.
[58] Z. X. Ng, D. Tan, W. L. Teo, F. León, X. Shi, Y. Sim, Y. Li, R. Ganguly, Y. Zhao, S. Mohamed *et al.*, Mechanosynthesis of higher-order cocrystals: Tuning order, functionality and size in cocrystal design, Angew. Chem. Int. Ed. **60**, 17481 (2021).
[59] J. Guo, Y. Zeng, Y. Zhen, H. Geng, Z. Wang, Y. Yi, H. Dong, and W. Hu, Non-equal ratio cocrystal engineering to improve charge transport characteristics of organic semiconductors: A case study on indolo[2,3-a]carbazole, Angew. Chem. Int. Ed. **61**, e202202336 (2022).
[60] Y. Wang, H. Wu, L. O. Jones, M. A. Mosquera, C. L. Stern, G. C. Schatz, and J. F. Stoddart, Color-tunable upconversion-emission switch based on cocrystal-to-cocrystal transformation, J. Am. Chem. Soc. **145**, 1855 (2023).
[61] J. Zhang, J. Tan, Z. Ma, W. Xu, G. Zhao, H. Geng, C. Di, W. Hu, Z. Shuai, K. Singh *et al.*, Fullerene/sulfur-bridged annulene cocrystals: Two-dimensional segregated heterojunctions with ambipolar transport properties and photoresponsivity, J. Am. Chem. Soc. **135**, 558 (2013).
[62] See Supplemental Material at http://link.aps.org/supplemental/10.1103/PhysRevE.109.064603 for futher details of the contact diagrams within various molecular crystals.